

# Study of Excited $\Xi_c$ States Decaying into $\Xi_c^0$ and $\Xi_c^+$ Baryons

J. Yelton,<sup>8</sup> I. Adachi,<sup>14,11</sup> H. Aihara,<sup>70</sup> D. M. Asner,<sup>54</sup> V. Aulchenko,<sup>3,53</sup> T. Aushev,<sup>44</sup> R. Ayad,<sup>63</sup> I. Badhrees,<sup>63,29</sup> S. Bahinipati,<sup>17</sup> A. M. Bakich,<sup>62</sup> E. Barberio,<sup>41</sup> P. Behera,<sup>19</sup> B. Bhuyan,<sup>18</sup> J. Biswal,<sup>25</sup> G. Bonvicini,<sup>74</sup> A. Bozek,<sup>50</sup> M. Bračko,<sup>39,25</sup> T. E. Browder,<sup>13</sup> D. Červenkóv,<sup>4</sup> A. Chen,<sup>47</sup> B. G. Cheon,<sup>12</sup> K. Chilikin,<sup>35,43</sup> K. Cho,<sup>30</sup> Y. Choi,<sup>61</sup> D. Cinabro,<sup>74</sup> M. Danilov,<sup>43,35</sup> N. Dash,<sup>17</sup> S. Di Carlo,<sup>74</sup> Z. Doležal,<sup>4</sup> Z. Drásal,<sup>4</sup> D. Dutta,<sup>64</sup> S. Eidelman,<sup>3,53</sup> H. Farhat,<sup>74</sup> J. E. Fast,<sup>54</sup> T. Ferber,<sup>7</sup> B. G. Fulsom,<sup>54</sup> V. Gaur,<sup>64</sup> N. Gabyshev,<sup>3,53</sup> A. Garmash,<sup>3,53</sup> R. Gillard,<sup>74</sup> P. Goldenzweig,<sup>27</sup> T. Hara,<sup>14,11</sup> K. Hayasaka,<sup>51</sup> H. Hayashii,<sup>46</sup> W.-S. Hou,<sup>49</sup> G. Inguglia,<sup>7</sup> A. Ishikawa,<sup>68</sup> R. Itoh,<sup>14,11</sup> Y. Iwasaki,<sup>14</sup> W. W. Jacobs,<sup>20</sup> H. B. Jeon,<sup>33</sup> D. Joffe,<sup>28</sup> K. K. Joo,<sup>5</sup> T. Julius,<sup>41</sup> K. H. Kang,<sup>33</sup> E. Kato,<sup>68</sup> Y. Kato,<sup>45</sup> D. Y. Kim,<sup>59</sup> J. B. Kim,<sup>31</sup> K. T. Kim,<sup>31</sup> S. H. Kim,<sup>12</sup> K. Kinoshita,<sup>6</sup> P. Kodyš,<sup>4</sup> S. Korpar,<sup>39,25</sup> D. Kotchetkov,<sup>13</sup> P. Krizan,<sup>36,25</sup> P. Krokovny,<sup>3,53</sup> T. Kumita,<sup>72</sup> A. Kuzmin,<sup>3,53</sup> Y.-J. Kwon,<sup>76</sup> J. S. Lange,<sup>9</sup> C. H. Li,<sup>41</sup> H. Li,<sup>20</sup> L. Li,<sup>57</sup> Y. Li,<sup>73</sup> J. Libby,<sup>19</sup> D. Liventsev,<sup>73,14</sup> M. Lubej,<sup>25</sup> T. Luo,<sup>55</sup> M. Masuda,<sup>69</sup> T. Matsuda,<sup>42</sup> D. Matvienko,<sup>3,53</sup> K. Miyabayashi,<sup>46</sup> H. Miyata,<sup>51</sup> R. Mizuk,<sup>35,43,44</sup> G. B. Mohanty,<sup>64</sup> A. Moll,<sup>40,65</sup> H. K. Moon,<sup>31</sup> T. Nanut,<sup>25</sup> K. J. Nath,<sup>18</sup> M. Nayak,<sup>74,14</sup> K. Negishi,<sup>68</sup> M. Niiyama,<sup>32</sup> S. Nishida,<sup>14,11</sup> S. Ogawa,<sup>67</sup> S. Okuno,<sup>26</sup> P. Pakhlov,<sup>35,43</sup> G. Pakhlova,<sup>35,44</sup> B. Pal,<sup>6</sup> C.-S. Park,<sup>76</sup> H. Park,<sup>33</sup> S. Paul,<sup>66</sup> T. K. Pedlar,<sup>38</sup> R. Pestotnik,<sup>25</sup> L. E. Pilonen,<sup>73</sup> C. Pulvermacher,<sup>27</sup> M. Ritter,<sup>37</sup> A. Rostomyan,<sup>7</sup> Y. Sakai,<sup>14,11</sup> S. Sandilya,<sup>6</sup> L. Santelj,<sup>14</sup> T. Sanuki,<sup>68</sup> V. Savinov,<sup>55</sup> T. Schlüter,<sup>37</sup> O. Schneider,<sup>34</sup> G. Schnell,<sup>1,16</sup> C. Schwanda,<sup>22</sup> Y. Seino,<sup>51</sup> K. Senyo,<sup>75</sup> O. Seon,<sup>45</sup> M. E. Sevior,<sup>41</sup> V. Shebalin,<sup>3,53</sup> C. P. Shen,<sup>2</sup> T.-A. Shibata,<sup>71</sup> J.-G. Shiu,<sup>49</sup> A. Sokolov,<sup>23</sup> E. Solovieva,<sup>35,44</sup> S. Stanič,<sup>52</sup> M. Starič,<sup>25</sup> J. F. Strube,<sup>54</sup> M. Sumihama,<sup>10</sup> T. Sumiyoshi,<sup>72</sup> M. Takizawa,<sup>58,15,56</sup> U. Tamponi,<sup>77,78</sup> K. Tanida,<sup>24</sup> F. Tenchini,<sup>41</sup> M. Uchida,<sup>71</sup> T. Uglov,<sup>35,44</sup> S. Uno,<sup>14,11</sup> P. Urquijo,<sup>41</sup> Y. Usov,<sup>3,53</sup> C. Van Hulse,<sup>1</sup> G. Varner,<sup>13</sup> A. Vinokurova,<sup>3,53</sup> C. H. Wang,<sup>48</sup> M.-Z. Wang,<sup>49</sup> P. Wang,<sup>21</sup> Y. Watanabe,<sup>26</sup> E. Widmann,<sup>60</sup> K. M. Williams,<sup>73</sup> E. Won,<sup>31</sup> C. Z. Yuan,<sup>21</sup> Z. P. Zhang,<sup>57</sup> V. Zhilich,<sup>3,53</sup> V. Zhukova,<sup>43</sup> V. Zhulanov,<sup>3,53</sup> and A. Zupanc<sup>36,25</sup>

(The Belle Collaboration)

<sup>1</sup>University of the Basque Country UPV/EHU, 48080 Bilbao

<sup>2</sup>Beihang University, Beijing 100191

<sup>3</sup>Budker Institute of Nuclear Physics SB RAS, Novosibirsk 630090

<sup>4</sup>Faculty of Mathematics and Physics, Charles University, 121 16 Prague

<sup>5</sup>Chonnam National University, Kwangju 660-701

<sup>6</sup>University of Cincinnati, Cincinnati, Ohio 45221

<sup>7</sup>Deutsches Elektronen-Synchrotron, 22607 Hamburg

<sup>8</sup>University of Florida, Gainesville, Florida 32611

<sup>9</sup>Justus-Liebig-Universität Gießen, 35392 Gießen

<sup>10</sup>Gifu University, Gifu 501-1193

<sup>11</sup>SOKENDAI (The Graduate University for Advanced Studies), Hayama 240-0193

<sup>12</sup>Hanyang University, Seoul 133-791

<sup>13</sup>University of Hawaii, Honolulu, Hawaii 96822

<sup>14</sup>High Energy Accelerator Research Organization (KEK), Tsukuba 305-0801

<sup>15</sup>J-PARC Branch, KEK Theory Center, High Energy Accelerator Research Organization (KEK), Tsukuba 305-0801

<sup>16</sup>IKERBASQUE, Basque Foundation for Science, 48013 Bilbao

<sup>17</sup>Indian Institute of Technology Bhubaneswar, Satya Nagar 751007

<sup>18</sup>Indian Institute of Technology Guwahati, Assam 781039

<sup>19</sup>Indian Institute of Technology Madras, Chennai 600036

<sup>20</sup>Indiana University, Bloomington, Indiana 47408

<sup>21</sup>Institute of High Energy Physics, Chinese Academy of Sciences, Beijing 100049

<sup>22</sup>Institute of High Energy Physics, Vienna 1050

<sup>23</sup>Institute for High Energy Physics, Protvino 142281

<sup>24</sup>Advanced Science Research Center, Japan Atomic Energy Agency, Naka 319-1195

<sup>25</sup>J. Stefan Institute, 1000 Ljubljana

<sup>26</sup>Kanagawa University, Yokohama 221-8686

<sup>27</sup>Institut für Experimentelle Kernphysik, Karlsruher Institut für Technologie, 76131 Karlsruhe

<sup>28</sup>Kennesaw State University, Kennesaw, Georgia 30144

<sup>29</sup>King Abdulaziz City for Science and Technology, Riyadh 11442

<sup>30</sup>Korea Institute of Science and Technology Information, Daejeon 305-806

<sup>31</sup>Korea University, Seoul 136-713

- <sup>32</sup> *Kyoto University, Kyoto 606-8502*
- <sup>33</sup> *Kyungpook National University, Daegu 702-701*
- <sup>34</sup> *École Polytechnique Fédérale de Lausanne (EPFL), Lausanne 1015*
- <sup>35</sup> *P.N. Lebedev Physical Institute of the Russian Academy of Sciences, Moscow 119991*
- <sup>36</sup> *Faculty of Mathematics and Physics, University of Ljubljana, 1000 Ljubljana*
- <sup>37</sup> *Ludwig Maximilians University, 80539 Munich*
- <sup>38</sup> *Luther College, Decorah, Iowa 52101*
- <sup>39</sup> *University of Maribor, 2000 Maribor*
- <sup>40</sup> *Max-Planck-Institut für Physik, 80805 München*
- <sup>41</sup> *School of Physics, University of Melbourne, Victoria 3010*
- <sup>42</sup> *University of Miyazaki, Miyazaki 889-2192*
- <sup>43</sup> *Moscow Physical Engineering Institute, Moscow 115409*
- <sup>44</sup> *Moscow Institute of Physics and Technology, Moscow Region 141700*
- <sup>45</sup> *Graduate School of Science, Nagoya University, Nagoya 464-8602*
- <sup>46</sup> *Nara Women's University, Nara 630-8506*
- <sup>47</sup> *National Central University, Chung-li 32054*
- <sup>48</sup> *National United University, Miao Li 36003*
- <sup>49</sup> *Department of Physics, National Taiwan University, Taipei 10617*
- <sup>50</sup> *H. Niewodniczanski Institute of Nuclear Physics, Krakow 31-342*
- <sup>51</sup> *Niigata University, Niigata 950-2181*
- <sup>52</sup> *University of Nova Gorica, 5000 Nova Gorica*
- <sup>53</sup> *Novosibirsk State University, Novosibirsk 630090*
- <sup>54</sup> *Pacific Northwest National Laboratory, Richland, Washington 99352*
- <sup>55</sup> *University of Pittsburgh, Pittsburgh, Pennsylvania 15260*
- <sup>56</sup> *Theoretical Research Division, Nishina Center, RIKEN, Saitama 351-0198*
- <sup>57</sup> *University of Science and Technology of China, Hefei 230026*
- <sup>58</sup> *Showa Pharmaceutical University, Tokyo 194-8543*
- <sup>59</sup> *Soongsil University, Seoul 156-743*
- <sup>60</sup> *Stefan Meyer Institute for Subatomic Physics, Vienna 1090*
- <sup>61</sup> *Sungkyunkwan University, Suwon 440-746*
- <sup>62</sup> *School of Physics, University of Sydney, New South Wales 2006*
- <sup>63</sup> *Department of Physics, Faculty of Science, University of Tabuk, Tabuk 71451*
- <sup>64</sup> *Tata Institute of Fundamental Research, Mumbai 400005*
- <sup>65</sup> *Excellence Cluster Universe, Technische Universität München, 85748 Garching*
- <sup>66</sup> *Department of Physics, Technische Universität München, 85748 Garching*
- <sup>67</sup> *Toho University, Funabashi 274-8510*
- <sup>68</sup> *Department of Physics, Tohoku University, Sendai 980-8578*
- <sup>69</sup> *Earthquake Research Institute, University of Tokyo, Tokyo 113-0032*
- <sup>70</sup> *Department of Physics, University of Tokyo, Tokyo 113-0033*
- <sup>71</sup> *Tokyo Institute of Technology, Tokyo 152-8550*
- <sup>72</sup> *Tokyo Metropolitan University, Tokyo 192-0397*
- <sup>73</sup> *Virginia Polytechnic Institute and State University, Blacksburg, Virginia 24061*
- <sup>74</sup> *Wayne State University, Detroit, Michigan 48202*
- <sup>75</sup> *Yamagata University, Yamagata 990-8560*
- <sup>76</sup> *Yonsei University, Seoul 120-749*
- <sup>77</sup> *INFN - Sezione di Torino, 10125 Torino*
- <sup>78</sup> *University of Torino, 10124 Torino*

Using a data sample of  $980 \text{ fb}^{-1}$  of  $e^+e^-$  annihilation data taken with the Belle detector operating at the KEKB asymmetric-energy  $e^+e^-$  collider, we report the results of a study of excited  $\Xi_c$  states that decay, via the emission of photons and/or charged pions, into  $\Xi_c^0$  or  $\Xi_c^+$  ground state charmed-strange baryons. We present new measurements of the masses of all members of the  $\Xi_c'$ ,  $\Xi_c(2645)$ ,  $\Xi_c(2790)$ ,  $\Xi_c(2815)$ , and  $\Xi_c(2980)$  isodoublets, measurements of the intrinsic widths of those that decay strongly, and evidence of previously unknown transitions.

PACS numbers: 14.20.Lq

## INTRODUCTION

The  $\Xi_c$  states consist of a combination of a charm quark, a strange quark, and an up or down quark [1]. The ground-state  $\Xi_c^0$  and  $\Xi_c^+$  have  $J^P = 1/2^+$  and no orbital angular momentum and, like the  $\Lambda_c^+$ , have a wave-function that is antisymmetric under interchange of the lighter quark flavors or spins. The two ground states are the only members of the group that decay weakly, and their masses, lifetimes, and many of their decay modes have been measured [2]. The  $\Xi_c$  states also exist in many angular momentum configurations of the constituent quarks, each as an isospin pair. These excited states have been found to decay either electromagnetically or strongly in three different general types of decay: to the  $\Xi_c$  ground states together with mesons and/or photons, to final states that include a  $\Lambda_c^+$  and a kaon [3–5], and to  $\Lambda D$  final states [6]. This paper concentrates on the measurements of the masses and widths of the five isospin pairs of excited  $\Xi_c$  baryons that include a ground-state  $\Xi_c$  in their decay chain. All five pairs under investigation have previously been discovered, but in general their masses and intrinsic widths have not been measured precisely.

In the Heavy Quark Symmetry (HQS) [7] picture, the  $\Xi_c$  baryons are the combination of a heavy (charm) quark and a light ( $us$  or  $ds$ ) di-quark. In the standard quark model, the first excited pair have, like the ground-states,  $J^P = 1/2^+$ , but in this case the quarks in the light di-quark are symmetric under interchange in a similar manner to the  $\Sigma$  and  $\Sigma_c$  baryons. These are known as  $\Xi'_c$  baryons. This isospin pair is the only one that, because of the small mass differences involved, decays electromagnetically. The  $\Xi'_c$  pair was first discovered by CLEO in 1999 [8], but there have been no high statistics measurements of its mass. When the same “symmetric” di-quark combines with the charm quark in a  $J^P = 3/2^+$  configuration, the particles are denoted as  $\Xi_c(2645)$ , and sometimes known as  $\Xi_c^*$ . These were first discovered by CLEO in 1995 [9] and 1996 [10], and subsequently confirmed by a series of other experiments.

In the HQS model of baryons, the first orbitally excited states have a unit of angular momentum between the heavy quark and the light di-quark, with a spin-zero configuration of the light di-quark. This yields a total spin associated with the light degrees of freedom of one unit. This one unit then combines with the heavy quark spin to make  $J^P = 1/2^-$  and  $J^P = 3/2^-$  isodoublets. These two isodoublets were discovered by CLEO [11, 12]; the lower mass ( $\Xi_c(2790)$ , with  $J^P = 1/2^-$ ) states were found in the mode  $\Xi'_c\pi$  and the higher mass ( $\Xi_c(2815)$ , with  $J^P = 3/2^-$ ) states in  $\Xi_c(2645)\pi$  combinations. Until now, no measurements of their intrinsic widths have been reported. The quark configurations of all these states have been identified purely by their masses and decay products, but they fit the expected patterns so well that their identification is not considered controversial. A fifth isodoublet of excited states, the  $\Xi_c(2980)$ , was discovered by Belle [3] and confirmed by BaBar [4] in the decay mode  $\Lambda_c^+ K^- \pi^+$ , and subsequently seen, also by Belle, in the mode  $\Xi_c(2645)\pi$  [13]. Its  $J^P$  value is not determined, nor can it be assigned trivially in the standard quark model. Higher mass  $\Xi_c$  excited states of unknown quark configuration have been found [3–5].

The aim of this analysis is to measure, with greater precision than before, the masses of the five isodoublets of excited  $\Xi_c$  baryons that decay with  $\Xi_c$  ground states in their decay products, to measure the intrinsic widths of the four of these five isodoublets that decay strongly, and to look for new transitions that can help the identification of these states. Knowing the masses of these particles more accurately is of both practical and theoretical interest, and measuring their widths can then lead to measurements of the matrix elements of their decays; by HQS, these matrix elements are also applicable to other excited charm and bottom baryons [7, 14].

This analysis uses a data sample of  $e^+e^-$  annihilations recorded by the Belle detector [15] operating at the KEKB asymmetric-energy  $e^+e^-$  collider [16]. It corresponds to an integrated luminosity of  $980 \text{ fb}^{-1}$ . The majority of these data were taken with the accelerator energy tuned for production of the  $\Upsilon(4S)$  resonance, as this is optimum for investigation of  $B$  decays. However, the  $\Xi_c$  particles in this analysis are produced in continuum charm production and are of higher momentum than those that are decay products of  $B$  mesons, so the dataset used in this analysis also includes the Belle data taken at beam energies corresponding to the other  $\Upsilon$  resonances and the continuum nearby.

## THE BELLE DETECTOR AND GROUND-STATE $\Xi_c$ RECONSTRUCTION

The Belle detector is a large solid-angle spectrometer comprising six sub-detectors: the Silicon Vertex Detector (SVD), the 50-layer Central Drift Chamber (CDC), the Aerogel Cherenkov Counter (ACC), the Time-of-Flight scintillation counter (TOF), the electromagnetic calorimeter, and the  $K_L$  and muon detector. A superconducting solenoid produces a 1.5 T magnetic field throughout the first five of these sub-detectors. The detector is described in detail elsewhere [15]. Two inner detector configurations were used. The first comprised a 2.0 cm radius beampipe and a 3-layer silicon vertex detector, and the second a 1.5 cm radius beampipe and a 4-layer silicon detector and a small-cell inner drift chamber.

In order to study  $\Xi_c$  baryons, we first reconstruct a large sample of ground-state  $\Xi_c^0$  and  $\Xi_c^+$  baryons with good signal-to-noise ratio. To obtain large statistics, we use many decay modes of the ground-states, each with specific

requirements on their decay products designed to suppress combinatorial backgrounds. The decay modes used are listed in Table I.

Final-state charged particles,  $\pi^\pm$ ,  $K^-$ , and  $p$ , are selected using the likelihood information from the tracking (SVD, CDC) and charged-hadron identification (CDC, ACC, TOF) systems into a combined likelihood,  $\mathcal{L}(h1 : h2) = \mathcal{L}_{h1}/(\mathcal{L}_{h1} + \mathcal{L}_{h2})$  where  $h1$  and  $h2$  are  $p$ ,  $K$ , and  $\pi$  as appropriate. In general, we require proton candidates to have  $\mathcal{L}(p : K) > 0.6$  and  $\mathcal{L}(p : \pi) > 0.6$ , kaon candidates to have  $\mathcal{L}(K : p) > 0.6$  and  $\mathcal{L}(K : \pi) > 0.6$ , and pions to have the less restrictive requirements of  $\mathcal{L}(\pi : K) > 0.2$  and  $\mathcal{L}(\pi : p) > 0.2$ . For one mode,  $\Xi_c^0 \rightarrow pK^-K^-\pi^+$ , the proton level is increased to 0.97 to ensure no contamination from charmed mesons. The  $\pi^0$  candidates are reconstructed from two detected neutral clusters in the ECL each consistent with being due to a photon and each with an energy greater than 50 MeV in the laboratory frame. The invariant mass of the photon pair is required to be within 3 standard deviations ( $\sigma$ ) of the nominal  $\pi^0$  mass. The same sample of photons is used for the  $\Sigma^0 \rightarrow \Lambda\gamma$  reconstruction. The  $\Lambda$  ( $K_S^0$ ) candidates are made from  $p\pi$  ( $\pi\pi$ ) pairs with a production vertex significantly separated from the interaction point (IP). For the case of the proton from the  $\Lambda$ , the particle identification is loosened to  $\mathcal{L}(p : K) > 0.2$  and  $\mathcal{L}(p : \pi) > 0.2$ . The  $\Lambda$  candidates used to directly reconstruct  $\Xi_c$  candidates are required to have an origin consistent with the IP, but those that are daughters of  $\Xi^-$ ,  $\Xi^0$  or  $\Omega^-$  candidates are not subject to this requirement.

The  $\Xi^-$  and  $\Omega^-$  candidates are made from the  $\Lambda$  candidates detailed above, together with a  $\pi^-$  or  $K^-$  candidate. The vertex formed from the  $\Lambda$  and  $\pi/K$  is required to be between the IP and the  $\Lambda$  decay vertex.

The  $\Xi^0$  and  $\Sigma^+$  reconstruction is complicated by the fact that the parent hyperon decays with a  $\pi^0$  (which has negligible vertex position information) as one of its daughters. In the case of the  $\Sigma^+ \rightarrow p\pi^0$  reconstruction, combinations of  $\pi^0$  candidates and protons are made using those protons with a significantly large ( $> 1$  mm) impact parameter with respect to the IP. Then, assuming the IP to be the origin, a  $\Sigma^+$  trajectory is assumed, and the intersection of this trajectory with the reconstructed proton trajectory found. This position is taken as the decay location of the  $\Sigma^+$  hyperon, and the  $\pi^0$  is then re-fit using this as its point of origin. Only those combinations with the decay location of the  $\Sigma^+$  indicating a positive  $\Sigma^+$  path length are retained. The  $\Xi^0$  is reconstructed along similar lines but, in this case, it is not necessary to require a large impact parameter with respect to the IP.

Mass requirements are placed on all the hyperons reconstructed, based on the canonical masses of these particles. The half-widths of the mass intervals, all of which correspond to approximately two standard deviations of the resolution, are (in MeV/ $c^2$ ), 8.0, 5.0, 3.5, 3.5, 8.0 and 3.5 for  $\Sigma^+$ ,  $\Xi^0$ ,  $\Xi^-$ ,  $\Omega^-$ ,  $\Sigma^0$ , and  $\Lambda$ , respectively; the particles are kinematically constrained to the nominal masses for further analysis.

To show the yield of the reconstructed  $\Xi_c^0$  and  $\Xi_c^+$  baryons, we plot the mass peaks in Figs. 1 and 2 as distributions of the “pull mass,” that is, the difference between the measured and nominal mass (2470.85 MeV/ $c^2$  and 2467.93 MeV/ $c^2$  for the  $\Xi_c^0$  and  $\Xi_c^+$ , respectively[2]), divided by the resolution. For these plots, we require the scaled momentum of  $x_p > 0.6$ , where  $x_p = p^*c/\sqrt{(s/4 - c^2m^2)}$ , and  $p^*$  is the momentum in the center of mass and  $s$  is the total center-of-mass energy squared. This cut is not part of the analysis chain as we prefer to place an  $x_p$  cut on the excited states; however, it serves to display the signal-to-noise ratio of our reconstructed ground-state baryons. We also show in Table I the signal and background yields in each decay mode, integrated in a  $\pm 2\sigma$  interval around the nominal mass.

Once the daughter particles of a  $\Xi_c$  candidate are selected, the  $\Xi_c$  candidate itself is made by kinematically fitting the daughters to a common decay vertex. The IP is not included in this vertex, as the small decay length associated with the  $\Xi_c$  decays, though very short compared with the  $\Xi^-$ ,  $\Xi^0$ ,  $\Omega^-$  and  $\Sigma^+$  decay lengths, is not completely negligible. The  $\chi^2$  of this vertex is required to be consistent with all the daughters being produced by a common parent.

The above reconstruction of  $\Xi_c$  baryons is optimized to have generally good efficiency and good signal-to-noise ratio for high momentum candidates. The identical sample is used for all the different analyses described below.

### THE $\Xi_c(2645)$ AND $\Xi_c(2815)$ ISODOUBLETS

The decay chain  $\Xi_c(2815) \rightarrow \Xi_c(2645)\pi$ ,  $\Xi_c(2645) \rightarrow \Xi_c\pi$  allows us to obtain samples of both the  $\Xi_c(2815)$  and  $\Xi_c(2645)$  states with excellent signal-to-noise ratio. The mass-constrained  $\Xi_c$  samples obtained as described above are combined with two appropriately charged pions not contributing to the reconstructed  $\Xi_c$ ; a vertex constraint of the three particles is made with the IP included to optimize the mass resolution. For each isospin state, all decay modes of the  $\Xi_c$  are considered together. We then place a requirement of  $x_p > 0.7$  on the  $\Xi_c(2815)$  candidate. This requirement is typical for studies of orbitally excited charmed baryons which are known to have hard fragmentation functions. The scatter plots of  $\Xi_c\pi\pi$  mass versus  $\Xi_c\pi$  mass show the significant  $\Xi_c(2815) \rightarrow \Xi_c(2645)\pi$  signals in both isospin states (Fig. 3).

To study the  $\Xi_c(2815)$  we place a requirement that the  $\Xi_c^0\pi^+$  ( $\Xi_c^+\pi^-$ ) combination be within  $\pm 5.0$  MeV/ $c^2$  of the  $\Xi_c(2645)$  mass peak (as shown by the lines in Fig. 3), and then make plots of the  $\Xi_c^0\pi^+\pi^-$  and  $\Xi_c^+\pi^-\pi^+$  mass (Fig. 4). In each case, a prominent peak is found in the expected region, with a low level of background.

TABLE I. The yield of each decay mode of the ground state  $\Xi_c^0$  and  $\Xi_c^+$  for  $x_p > 0.6$ . The yields and background are found by integrating over a range of  $\pm 2\sigma$  around the peak value, where  $\sigma$  is the resolution. Note that this  $x_p$  cut is not part of the analysis.

Mode	Signal yield ( $10^3$ )	Background yield ( $10^3$ )
$\Omega^- K^+$	4.3	0.4
$\Xi^- \pi^+$	24.3	6.5
$\Xi^- \pi^+ \pi^- \pi^+$	9.6	9.8
$\Lambda K^- \pi^+$	15.7	11.3
$p K^- K^- \pi^+$	9.5	6.5
$\Xi^- \pi^+ \pi^0$	15.8	13.2
$\Xi^0 \pi^+ \pi^+$	3.7	3.4
$\Lambda K_S^0$	4.8	5.0
$p K^- K_S^0$	6.4	10.6
$\Sigma^0 K^- \pi^+$	6.7	4.3
Sum of above $\Xi_c^0$ modes	100.8	71.0
$\Xi^- \pi^+ \pi^+$	33.6	8.8
$\Lambda K^- \pi^+ \pi^+$	5.0	3.4
$\Xi^0 \pi^+$	1.4	1.1
$\Xi^0 \pi^+ \pi^- \pi^+$	2.5	2.4
$\Sigma^+ K^- \pi^+$	6.0	3.5
$\Lambda K_S^0 \pi^+$	6.5	7.4
$\Sigma^0 K_S^0 \pi^+$	1.1	1.5
Sum of above $\Xi_c^+$ modes	56.1	28.1

These two distributions are fit to signal functions comprising Breit-Wigner functions convolved with double-Gaussian resolution functions and first-order polynomial backgrounds. For this and all other distributions in this analysis, the resolution function is obtained from Monte Carlo (MC) events, generated using EvtGen [17] with the Belle detector response simulated using the GEANT3 [18] framework. The widths of the resolution functions are expressed as weighted averages of the components of the double Gaussian, and are shown in Table II. The fitted masses are  $(2819.98 \pm 0.08)$  MeV/ $c^2$  and  $(2816.62 \pm 0.09)$  MeV/ $c^2$  for the  $\Xi_c^+(2815)$  and  $\Xi_c^0(2815)$ , respectively, and the widths are  $\Gamma(\Xi_c^+(2815)) = (2.34 \pm 0.18)$  MeV and  $\Gamma(\Xi_c^0(2815)) = (2.31 \pm 0.20)$  MeV; in all cases, the quoted uncertainty is only statistical.

The Belle momentum scale has been studied using the masses of well-measured parent particles as reference points. Close inspection shows small biases in the momentum measurement of low momentum tracks which can lead to a small mis-measurement of mass peaks found using charged pion transitions and systematic shifts in the measured mass of the excited states under investigation here.

High-statistic studies of the  $M(D^{*+}) - M(D^0)$  mass difference measured in  $D^{*+} \rightarrow D^0 \pi^+$  decay as a function of the momentum of the transition pion [19] show deviations from the expected mass difference that are attributed to limitations in the accuracy with which the track-fitting programs take into account the detector material. These limitations are reproduced in the Monte Carlo modeling. In the analyses described here, these small biases are thus taken into account by assigning a correction of a fraction of an MeV/ $c^2$  to the measured masses of all the strongly decaying resonances under consideration, using the Monte Carlo programs to evaluate these corrections. These corrections have already been applied in the masses for the  $\Xi_c(2815)$  states quoted above, and are listed in Table II. The systematic uncertainties assigned to these corrections are discussed further below and final results including systematic uncertainties shown in Table IV.

Relaxing the mass cut around the  $\Xi_c(2645)$  peaks and instead selecting events in the  $\Xi_c \pi \pi$  spectrum within 6 MeV/ $c^2$  of the  $\Xi_c(2815)$  signal, we can study the  $\Xi_c^0 \pi^+$  and  $\Xi_c^+ \pi^-$  mass spectra (Fig. 5). Using this method of selection, rather than looking at these combinations inclusively, produces  $\Xi_c(2645)$  signals of much higher signal-to-noise ratio than is possible in inclusive studies [5], and reduces the dependence on the shape of the background, which is especially important as any background may include “satellite” peaks from partially reconstructed resonances. The two distributions are fit, as in the case of the  $\Xi_c(2815)$ , to obtain masses of  $(2645.44 \pm 0.06)$  MeV/ $c^2$  for the  $\Xi_c^+(2645)$  and  $(2646.32 \pm 0.07)$  MeV/ $c^2$  for the  $\Xi_c^0(2645)$ , with intrinsic widths of  $\Gamma(\Xi_c^+(2645)) = (2.04 \pm 0.14)$  MeV and  $\Gamma(\Xi_c^0(2645)) = (2.26 \pm 0.18)$  MeV, where the uncertainties quoted are statistical only, and the systematic uncertainties discussed in section on systematic uncertainties. We note that the requirements of 5 MeV/ $c^2$  and 6 MeV/ $c^2$  detailed above are sufficiently loose to not significantly bias the subsequent measurements.

TABLE II. The width of the Monte Carlo derived resolution functions, expressed as a weighted average in quadrature of the two standard deviations that comprise the double-Gaussian functions used, and the mass offsets derived from Monte Carlo.

Mode	Resolution ( $\sigma_{\text{av}}(\text{MeV}/c^2)$ )	Monte Carlo $M_{\text{rec}} - M_{\text{gen}}(\text{MeV}/c^2)$
$\Xi_c(2645) \rightarrow \Xi_c \pi$	0.82	-0.07
$\Xi_c(2815) \rightarrow \Xi_c \pi \pi$	1.15	-0.12
$\Xi_c(2980) \rightarrow \Xi_c \pi \pi$	1.99	-0.28
$\Xi'_c \rightarrow \Xi_c \gamma$	5.5	+0.36
$\Xi_c(2790) \rightarrow \Xi'_c \pi$	1.34	-0.12
$\Xi_c(2815) \rightarrow \Xi'_c \pi$	1.58	-0.17
$\Xi_c(2980) \rightarrow \Xi'_c \pi$	1.90	-0.23

### THE $\Xi_c(2980) \rightarrow \Xi_c(2645)\pi$ DECAY

The  $\Xi_c(2980)$  state was discovered in  $\Xi_c(2645)\pi$  decay by Belle in 2005 [3], and then found to also decay to  $\Lambda_c^+ K^- \pi^+$  [13]. The analysis of this state is identical to that of the  $\Xi_c(2815)$  above except that we focus on the mass range 2.84-3.10  $\text{GeV}/c^2$  and present the mass distributions (Fig. 6) in bins appropriate for the width of the signal. We choose not to try to fit the mass range extending from below the  $\Xi_c(2815)$  to the  $\Xi_c(2980)$  with one fit, as the background shape may include undulations due to combinations of partially reconstructed excited  $\Xi_c$  states with other pions.

As in the previous case, the signal shape is a Breit-Wigner convolved with a double-Gaussian resolution function. This gives signal yields as shown in Table I. The measured masses and widths are  $M(\Xi_c^0(2980)) = (2970.8 \pm 0.7) \text{ MeV}/c^2$ ,  $M(\Xi_c^+(2980)) = (2966.0 \pm 0.8) \text{ MeV}/c^2$ ,  $\Gamma(\Xi_c^0(2980)) = (30.3 \pm 2.3) \text{ MeV}$ ,  $\Gamma(\Xi_c^+(2980)) = (28.1 \pm 2.6) \text{ MeV}$ , where the uncertainties shown are purely statistical.

### THE $\Xi'_c \rightarrow \Xi_c$ DECAY

The  $\Xi'_c$  doublet is the charmed-strange analog of the  $\Sigma_c(2455)$  triplet. However, because their mass difference with respect to the ground state is less than the pion mass, the  $\Xi'_c$  particles are found by their electromagnetic decays,  $\Xi'_c \rightarrow \Xi_c \gamma$ , and their intrinsic widths are experimentally negligible. The photons, detected in the electromagnetic calorimeter, are required to have an energy greater than 100 MeV in the laboratory frame, and to have a transverse shape consistent with that expected for a single photon. Each photon is combined with the  $\Xi_c$  candidates, as detailed above, and the  $\Xi_c \gamma$  mass distribution is plotted for combinations with a value of  $x_p > 0.65$ . This lower choice of the  $x_p$  requirement is because the  $\Xi'_c$  is not orbitally excited and is often a decay product of higher-mass states. The shape of the background is complicated by the fact that the low energy threshold allows many fake photons, not necessarily emanating from the collision, to be included. There are clearly many  $\pi^0$  transitions from excited  $\Xi_c$  states that produce photons correlated with the ground-state  $\Xi_c$  baryons. It is not possible to improve the signal and background separation by vetoing photons that can be combined with another photon to make a  $\pi^0$ , as the number of fake photons is too high.

The  $\Xi_c \gamma$  mass distributions (Fig. 7) are fit to the sum of a polynomial background function and two ‘‘Crystal Ball’’ [20] functions to parameterize the signal. The Crystal Ball function is a Gaussian with an exponential tail on the low mass end. In this case we add two Crystal Ball functions in a fixed ratio with differing Gaussian resolution components but all other parameters, derived using Monte Carlo modeling, at fixed values. The asymmetry of the functional form naturally leads to a mass shift, whereby the most likely mass is not the same as the peak mass found from the fit. This effect is modeled in Monte Carlo, and results in a  $0.36 \text{ MeV}/c^2$  shift. The measured masses, taking into account this shift, are  $(2579.2 \pm 0.1) \text{ MeV}/c^2$  and  $(2578.4 \pm 0.1) \text{ MeV}/c^2$  for the  $\Xi_c^{\prime+}$  and  $\Xi_c^{\prime0}$ , respectively, where the uncertainties are statistical only; the systematic uncertainties are discussed below.

### STUDY OF $\Xi'_c \pi$ COMBINATIONS

The  $\Xi'_c$  candidates detailed above are mass-constrained to their measured mass values, and then the combinations of these candidates with appropriately charged pions in the events are made to search for excited resonances decaying to  $\Xi_c^0 \pi^+$  or  $\Xi_c^+ \pi^-$ .

The mass distributions for these combinations, with a requirement of  $x_p > 0.7$ , are shown in Fig. 8, and both show large  $\Xi_c(2790)$  peaks and smaller peaks in the  $\Xi_c(2815)$  region. The low-mass cut-offs of the mass ranges were chosen

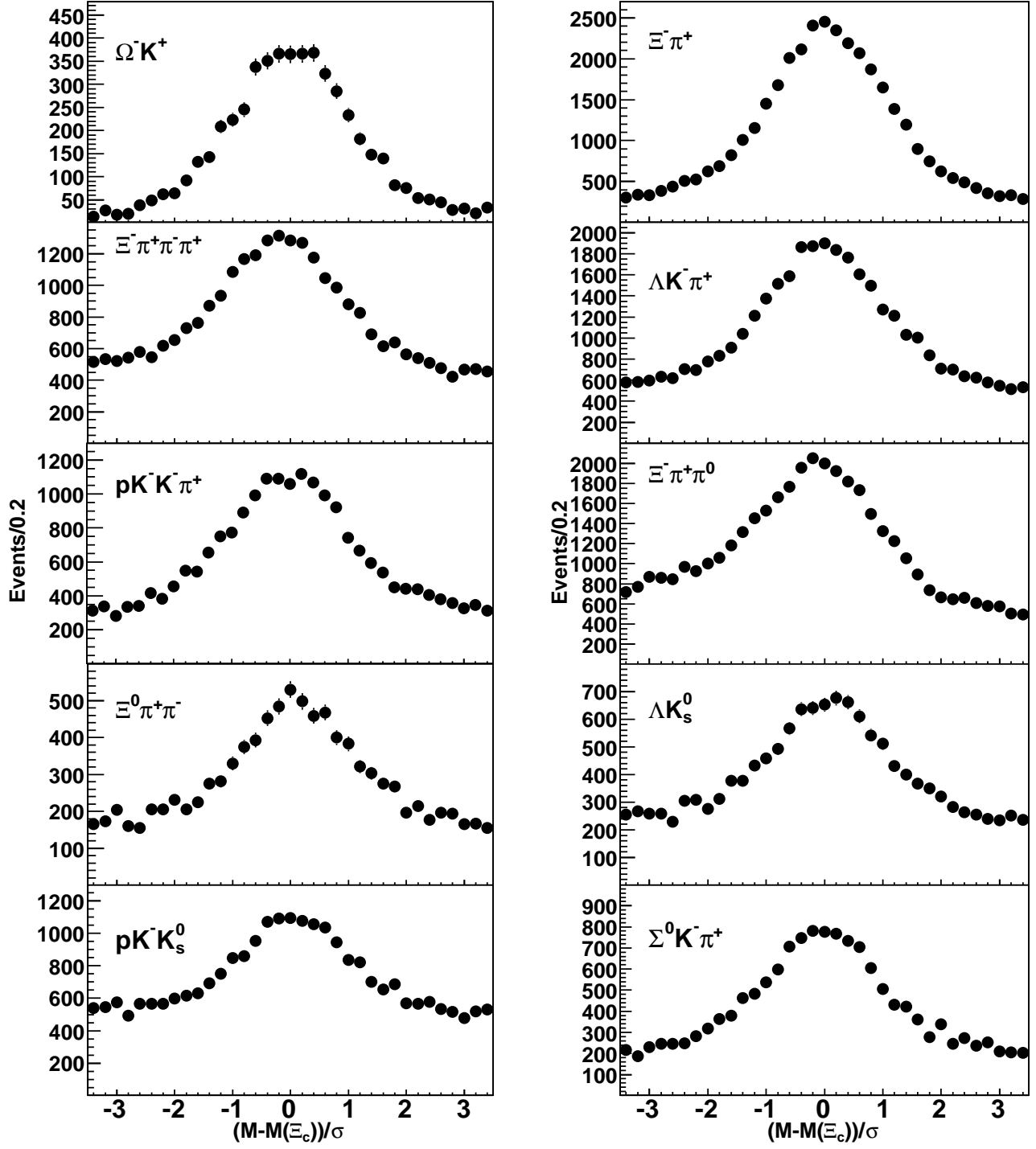


FIG. 1. The distribution of the “pull mass,” *i.e.*  $(M_{\text{measured}} - M(\Xi_c^0))/\sigma$ , for the ten  $\Xi_c^0$  modes used in this analysis. There is an  $x_p > 0.6$  requirement applied for presentation purposes, but this is not part of the analysis chain.

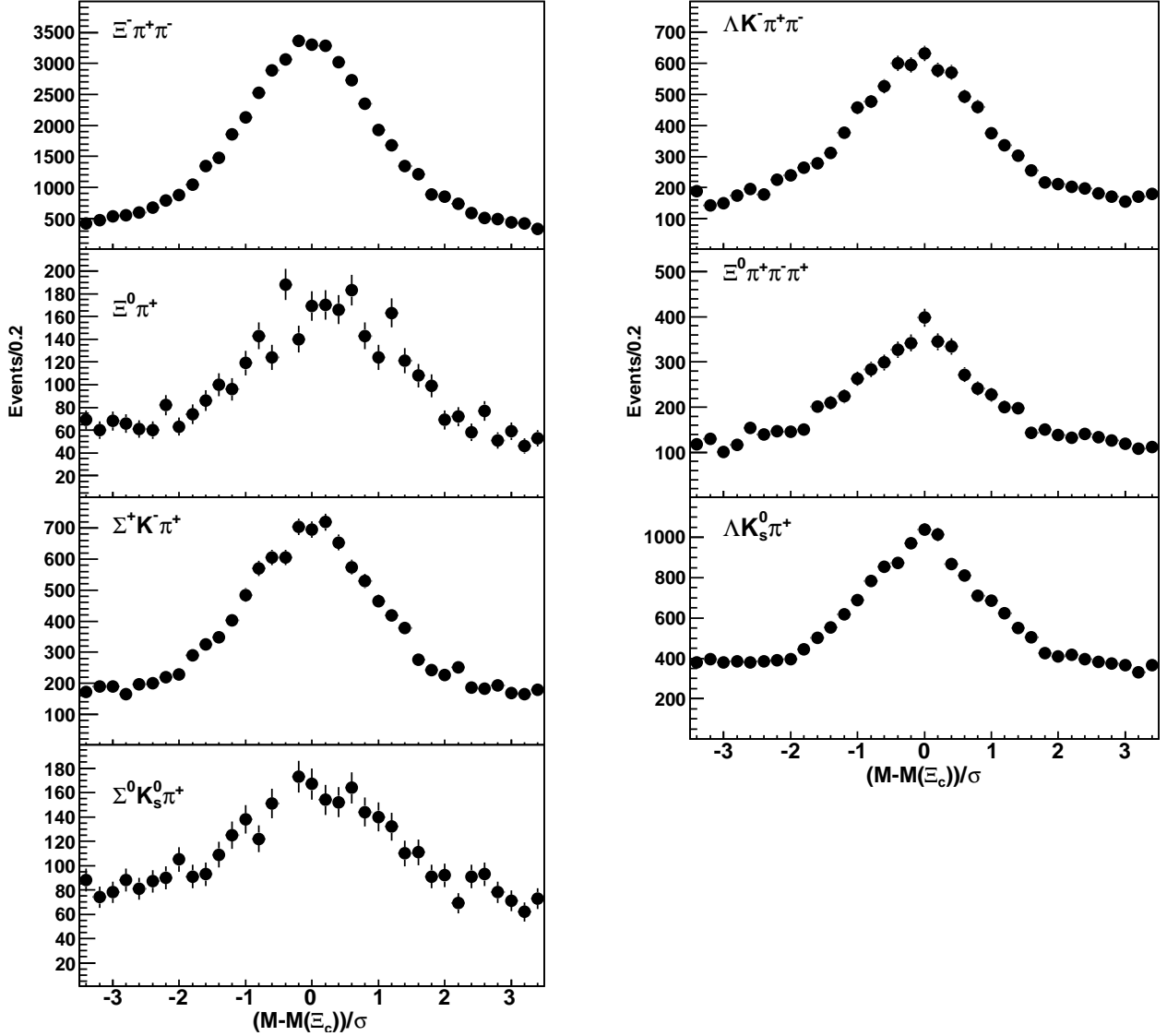


FIG. 2. The distribution of the “pull mass,” *i.e.*  $(M_{\text{measured}} - M(\Xi_c^+))/\sigma$ , for the seven  $\Xi_c^+$  modes used in this analysis. There is an  $x_p > 0.6$  requirement applied for presentation purposes, but this is not part of the analysis chain.

to exclude the satellite peaks found from fake  $\Xi_c'$  combinations with a transition pion from a  $\Xi_c(2645) \rightarrow \Xi_c$  decay. It is possible for background photons, particularly of low energy, to combine with the  $\Xi_c$  ground states to make  $\Xi_c'$  candidates. Once constrained to the  $\Xi_c'$  mass, several such candidates in one event can combine with a pion from a higher state to make multiple entries in this plot, all at similar total masses. To avoid this, we require that if there are multiple  $\Xi_c'$  candidates of this type in an event, only the one with an unconstrained mass closest to the  $\Xi_c'$  mass is considered. This reduces the overall population of the plot by around 15%.

Each distribution is fit to the sum of a polynomial background function, and two signal shapes. The signal shapes are each Breit-Wigners convolved with a double-Gaussian resolution function (as shown in Table II) to parameterize the  $\Xi_c(2790) \rightarrow \Xi_c'$  and  $\Xi_c(2815) \rightarrow \Xi_c' \pi$  decays. The masses and intrinsic widths of the  $\Xi_c(2815)$  states are fixed to those found in the analysis detailed above.

The masses and the widths of the  $\Xi_c(2790)$  states, with appropriate corrections as described above, are found to be  $M(\Xi_c^+(2790)) = (2791.6 \pm 0.2) \text{ MeV}/c^2$  and  $\Gamma(\Xi_c^+(2790)) = (8.9 \pm 0.6 \pm 0.8) \text{ MeV}$ , and  $M(\Xi_c^0(2790)) = (2794.9 \pm 0.3) \text{ MeV}/c^2$  and  $\Gamma(\Xi_c^0(2790)) = (10.0 \pm 0.7 \pm 0.8) \text{ MeV}$ . This is the first observation of significantly non-zero widths for these particles, although the original CLEO paper [11] indicated that it was likely that they had intrinsic widths of this order. The estimation of the systematic uncertainties on the masses follows the method used for the other states



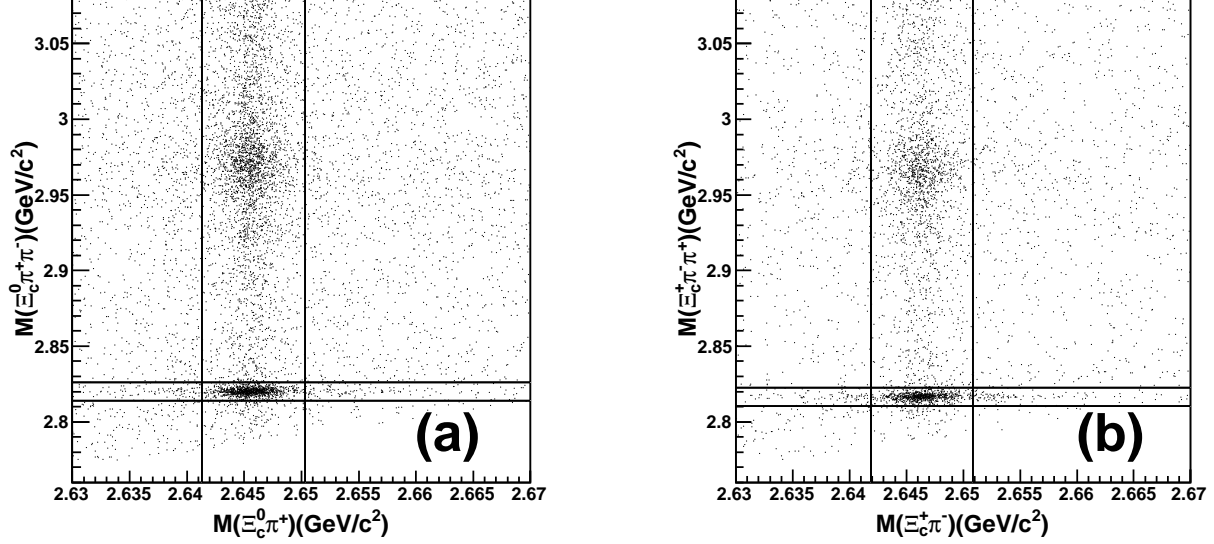


FIG. 3. Scatter plots of  $M(\Xi_c \pi \pi)$  versus  $M(\Xi_c(2645))$  for a)  $\Xi_c^0$  and b)  $\Xi_c^+$ . The lines show the positions of the requirements around the mass peaks used for projections on to the other axis.

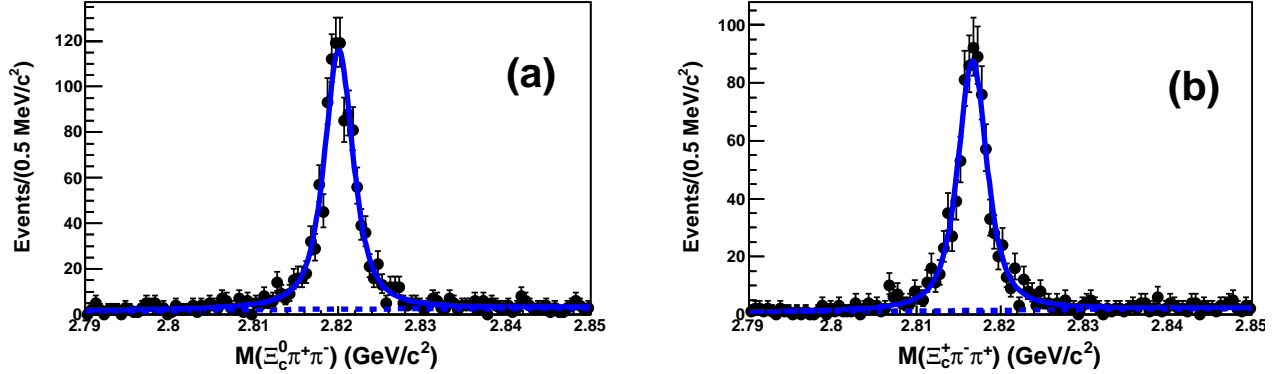


FIG. 4. The a)  $\Xi_c^0 \pi \pi$  and b)  $\Xi_c^+ \pi \pi$  invariant mass distributions with a cut on  $\Xi_c(2645)$  invariant mass of the intermediate state and a scaled momentum requirement of  $x_p > 0.7$ . Both show significant  $\Xi_c(2815)$  signals. The fits are described in the text. The dashed lines represent the combinatorial background contributions.

under investigation, and is described below. In this case, there is a systematic uncertainty due to the uncertainty in the  $M(\Xi_c') - M(\Xi_c)$  mass difference, as well as the uncertainties in the masses of the ground states.

Yields of  $128 \pm 25 \Xi_c^+(2815) \rightarrow \Xi_c^0 \pi^+$  events and  $52 \pm 17 \Xi_c^0(2815) \rightarrow \Xi_c^+ \pi^-$ , events are obtained. The central values of the corresponding mass peaks have an uncertainty as we are using the mass measurement via a decay chain into the neutral ground state to study the decay into the charged ground state, and vice versa.

It is not possible, from this study, to extract the branching ratio  $B(\Xi_c(2815) \rightarrow \Xi_c' \pi)/B(\Xi_c(2815) \rightarrow \Xi_c(2645) \pi)$  as we do not know the relative production cross sections of the ground-state  $\Xi_c$  baryons, or their absolute branching fraction in any one mode. However, we can perform a “back-of-the-envelope” calculation on the assumption that the efficiency times the branching fractions for the reconstructed modes of the two ground states indicated are equal to the ratio of those reconstructed, which is equivalent to assuming that the ground-state  $\Xi_c^0$  and  $\Xi_c^+$  are produced in equal numbers. Using this, we can infer that  $B(\Xi_c^+(2815) \rightarrow \Xi_c^0 \pi^+)/B(\Xi_c^+(2815) \rightarrow \Xi_c^0(2645) \pi^+, \Xi_c^0(2645) \rightarrow \Xi_c^+ \pi^-) \approx 11\%$ , and  $B(\Xi_c^0(2815) \rightarrow \Xi_c^+ \pi^-)/B(\Xi_c^0(2815) \rightarrow \Xi_c^+(2645) \pi^-, \Xi_c^+(2645) \rightarrow \Xi_c^0 \pi^+) \approx 10\%$ . In each of these branching fractions, the denominator and numerator involve different matrix elements [7].

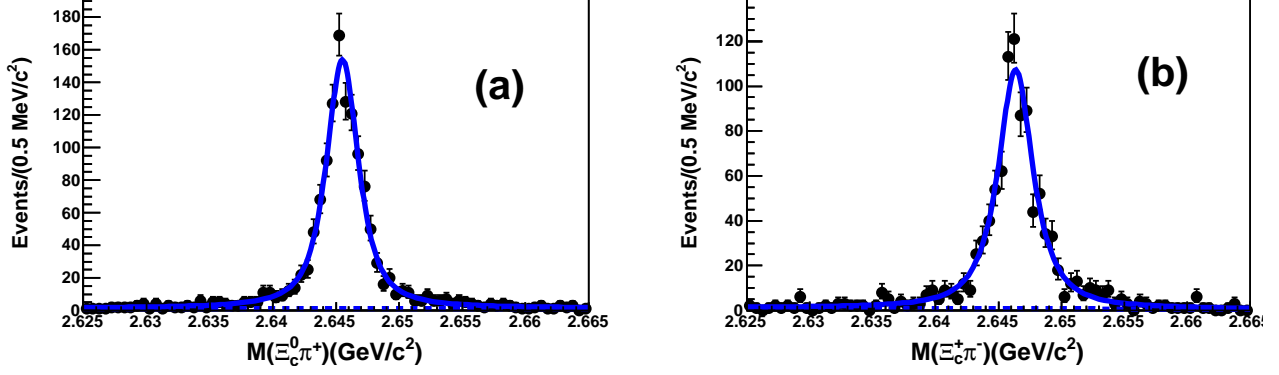


FIG. 5. The a)  $\Xi_c^0\pi^+$  and b)  $\Xi_c^+\pi^-$  invariant mass distributions with a selection on the  $\Xi_c\pi\pi$  invariant mass of the  $\Xi_c(2815)$  parent state and a scaled momentum cut of  $x_p > 0.7$  on the parent state. Both show clear  $\Xi_c(2645)$  signals. The fits are described in the text. The dashed lines represent the combinatorial background contributions.

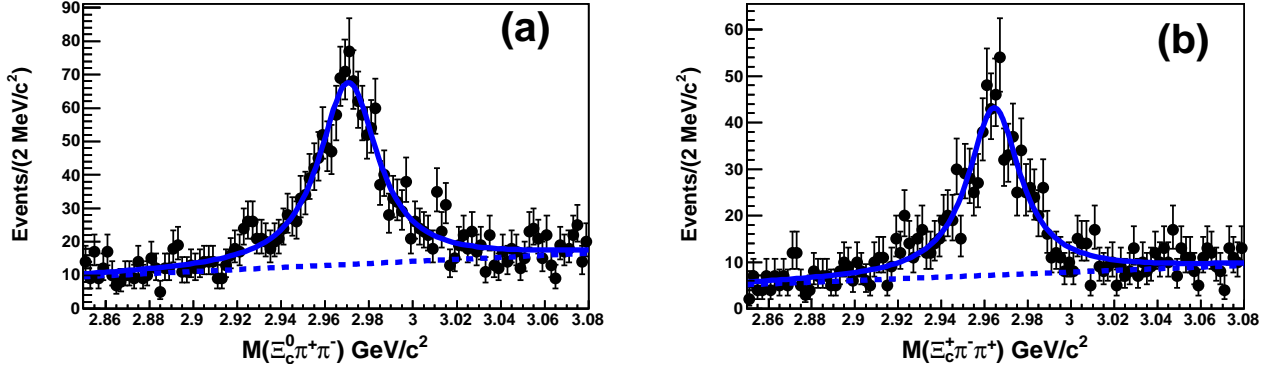


FIG. 6. The a)  $\Xi_c^0\pi^+\pi^-$  and b)  $\Xi_c^+\pi^-\pi^-$  invariant mass distributions with a cut on  $\Xi_c(2645)$  invariant mass of the intermediate state and a scaled momentum cut of  $x_p > 0.7$ . Both show clear  $\Xi_c(2980)$  signals. The fits are described in the text. The dashed lines represent the combinatorial background contributions.

### OBSERVATION OF $\Xi_c(2980) \rightarrow \Xi_c'\pi$ DECAYS

Lastly, we search for decays of the type  $\Xi_c(2980) \rightarrow \Xi_c'\pi$ . Figure 9 shows the same distributions as Fig. 8, plotted in a different mass region. We fit each distribution to the sum of a linear background function and signal functions using masses and intrinsic widths from our measurements above, and convolved with double-Gaussian resolution functions. The fitted yields are  $845 \pm 77$  and  $276 \pm 59$ , for the charged and neutral parent states, respectively.

Once again, we cannot accurately measure the relative branching fractions, but can estimate that  $B(\Xi_c^+(2980) \rightarrow \Xi_c^0\pi^+)/B(\Xi_c^+(2815) \rightarrow \Xi_c^0(2645)\pi^+, \Xi_c^0(2645) \rightarrow \Xi_c^+\pi^-) \approx 75\%$ , and  $B(\Xi_c^0(2980) \rightarrow \Xi_c^+\pi^-)/B(\Xi_c^0(2815) \rightarrow \Xi_c^+(2645)\pi^-, \Xi_c^+(2645) \rightarrow \Xi_c^0\pi^+) \approx 50\%$ . The apparently large branching fraction of the  $\Xi_c(2980)$  into  $\Xi_c'$  may prove useful in identifying the nature of the state. It does appear to be consistent with the decays of the  $\Lambda_c(2765)$  [21, 22], which is of similar excitation energy above its ground state. One possible interpretation is that they are radial excitations of the ground-state charmed baryons [23].

### SYSTEMATIC UNCERTAINTIES

In general, the resolution of the masses of resonances decaying via transition pions is dominated by the resolution of the momentum measurements of those pions rather than that of the ground states. However, Monte Carlo simulation predicts that decays to the different decay modes of the ground-state  $\Xi_c$  and  $\Xi_c'$  can have resolutions varying by  $\approx \pm 10\%$  of the average value. Therefore, in finding the resolution functions to be used, care is taken to generate the

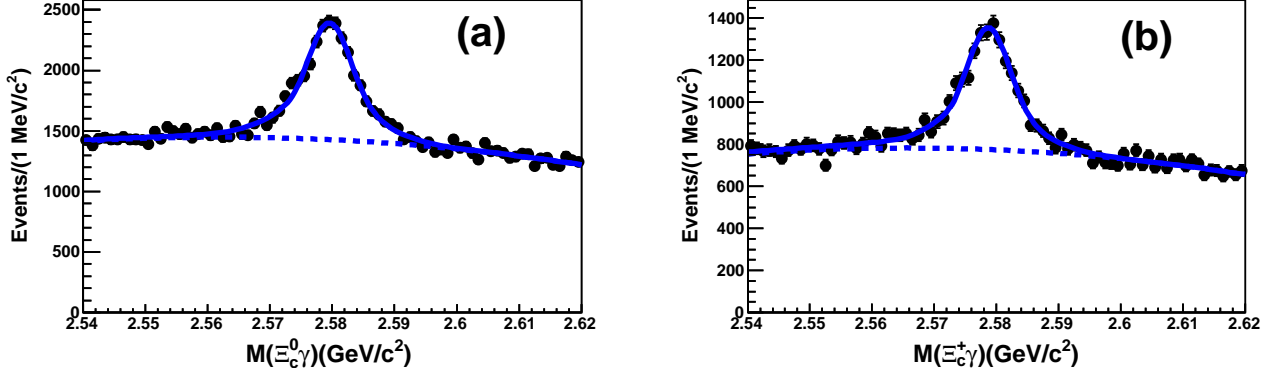


FIG. 7. The a)  $\Xi_c^0 \gamma$  and b)  $\Xi_c^+ \gamma$  invariant mass distributions. The fits are described in the text. The dashed lines represent the combinatorial background contributions.

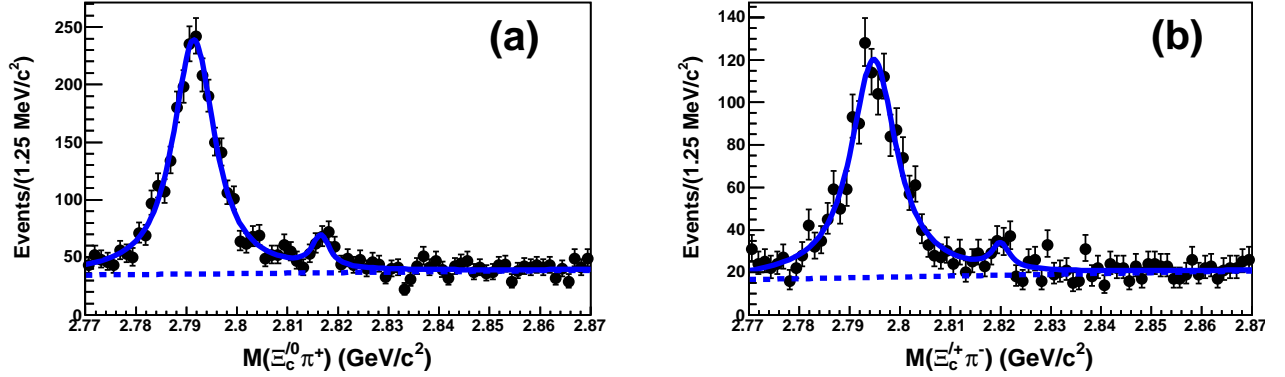


FIG. 8. The a)  $\Xi_c^0 \pi$  and b)  $\Xi_c^+ \pi$  invariant mass distributions. The fits are described in the text. The dashed lines represent the combinatorial background contributions.

various decay modes in the correct proportions to correctly reproduce the fractions found in the data. The events were also generated using the same range of beam energies as the real data, and with a fragmentation function (*i.e.*  $x_p$  distribution) that matches the data, as the resolution does vary slowly with momentum (with a change of  $\approx 10\%$  for the full momentum range under consideration).

A variety of checks are performed to ensure that the Monte Carlo generation technique was a good representation of the reconstructed data. For the final result on the masses of the particles, we separate the systematic uncertainty of the measurement of the mass differences, which is in effect what we are measuring, from that of the masses of the ground states tabulated by the Particle Data Group [2]. The overall momentum scale of the Belle detector is well studied from checks with  $K_S^0$  and other particle masses accurately known from other experiments. However, detailed studies of the  $D^{*+} \rightarrow D^0 \pi^+$  decay indicates that there are deviations particularly associated with the reconstruction and fitting of low-momentum charged tracks. As has been described above, this does lead to small systematic offsets in the found masses, and so the results are corrected for these effects. The uncertainty in these corrections is conservatively set at 50% of the offset, and these are listed as the uncertainty due to the mass scale in Table III.

The resolution in the Monte Carlo simulation matches the measured resolution within 8% for all the ground-state  $\Xi_c$  decay modes presented here. Further tests, specifically on the measurement of mass differences, were performed using the  $D^{*+} \rightarrow D^0 \pi^+$  and the  $\Lambda_c(2625) \rightarrow \Lambda_c^+ \pi^+ \pi^-$  decays. The latter uses an analysis chain very similar to the ones under consideration in this analysis, and, by matching the signal in the data with that in Monte Carlo simulated data with zero intrinsic width, we can conclude that the calculated width of the resolution cannot be more than 5% too broad for this topology. After assessment of the results of all of the above and other checks on the resolution, we assign a 10% uncertainty to the width of the resolution function, and assign the systematic uncertainties on the intrinsic widths accordingly.

All signal shapes used to analyze the strong decay transitions are Breit-Wigner functions convolved with double-Gaussian resolution functions. Technically, this is performed using two “Voigtian” functions in the RooFit fitting

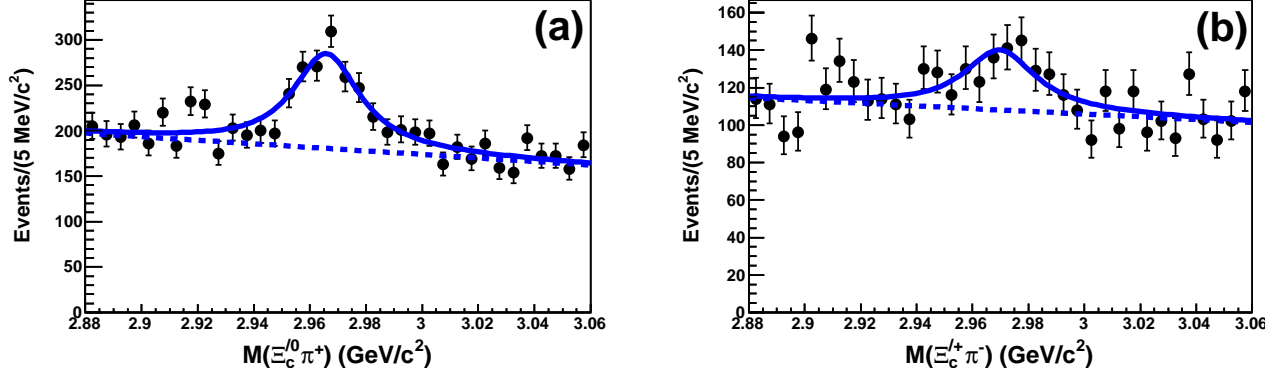


FIG. 9. The a)  $\Xi_c^0 \pi^+$  and b)  $\Xi_c'^+ \pi^-$  invariant mass distributions. The fits are described in the text. The dashed lines represent the combinatorial background contributions.

package [24]. Likelihood fits were performed using a large number of small bins - but are presented with bin sizes appropriate for each individual plot - so that there are negligible uncertainties associated with binning. Fits are also performed using relativistic Breit-Wigner functions that include spin-dependent and mass-dependent widths. As the widths of the particles are small compared with the  $Q^2$  associated with the decays, the extracted masses and widths do not depend greatly on the choice of signal functions. However, the small differences were considered as the systematic uncertainties associated with the signal shape. We do not use the relativistic Breit-Wigner functions for the default fits, as the spin-parity of the states have not been determined and, in addition, there are complications in the phase-space description of the decays when the decay product is itself of non-negligible intrinsic width.

The combinatorial backgrounds are parameterized by low-order Chebyshev polynomials. The small variations found by varying the order of this polynomial by one are taken as the systematic uncertainty due to the choice of background function. There is a specific issue with the background parameterization for the  $\Xi_c(2980)$  mass distribution of Fig. 6. Here, there is some evidence for peaking at around  $M = 2.92 \text{ GeV}/c^2$ , particularly in the neutral state. This evidence is not sufficient to claim the existence of a new particle, and may be an unidentified “satellite” peak formed from partially reconstructed resonances. Allowing an additional signal function to appear near this value changes the extracted width and mass values, lowering the extracted width measurement. This is particularly the case in the charged state, even though the evidence of a non-polynomial background shape is less convincing. These possible changes in values were considered part of the systematic uncertainty due to the background parameterization.

One of many checks on the photon energy scale, and the corrections made because of the asymmetric line-shape, was the reconstruction of  $D^{*0} \rightarrow D^0 \gamma$  using a very similar analysis. The measured mass difference was found to be  $0.15 \pm 0.10 \text{ MeV}$  higher than the Particle Data Group value [2], which is dominated by measurements using the low  $Q^2$  decay  $D^{*0} \rightarrow D^0 \pi^0$ . The assigned systematic uncertainty of  $0.4 \text{ MeV}$  for the  $\Xi_c'^+$  and  $\Xi_c^0$  mass differences with respect to the ground state is greater than this small discrepancy.

In Table III, we summarize the systematic uncertainties for the mass and width measurements of the five isodoublets under study. With the exception of the particular case of the background shape for the  $\Xi_c(2980)$  discussed above, if the method used to evaluate these uncertainties yields slightly different values for the two charged states, the greater of the two is used.

## RESULTS

Table IV shows the results of the measurements of the masses and widths of the five isodoublets. In all cases, the first uncertainty is statistical, and the second is the systematic uncertainty associated with the individual measurement. All the masses have a final, asymmetric uncertainty, taken from the Particle Data Group [2], for the mass of the ground states, and the  $\Xi_c(2790)$  have an extra uncertainty due to the uncertainty in the  $M(\Xi_c') - M(\Xi_c)$  measurement. The results are presented in this manner so that the final masses may be adjusted should new measurements on the ground states become available.

The systematic uncertainties associated with the mass scales cancel in the measurement of isospin splittings. However, in each case, there is an uncertainty that arises from the measurement of splitting of the ground states,  $M(\Xi_c^+) - M(\Xi_c^0) = (-2.92 \pm 0.48) \text{ MeV}/c^2$ . This is reported separately from the statistical and systematic uncertainties associated with this measurement so that the total uncertainties may be reduced when new measurements

TABLE III. The systematic uncertainties for the mass (in  $\text{MeV}/c^2$ ) and width measurements (in MeV). “Mass scale” refers to the uncertainty in making a mass measurement in the particular kinematic region under investigation. “Resolution” refers to uncertainty in the Monte Carlo correctly modeling the mass resolution, “Signal shape” refers to which version of a Breit-Wigner shape is used, and “Background Shape” refers to the uncertainty due to the use of different acceptable formulisms of the combinatorial background. The total systematic uncertainty is the quadratic sum of the individual contributions.

	Mass scale	Resolution	Signal shape	Background shape	Total
$M(\Xi_c(2645))$	0.04	0.0	0.06	0.01	0.07
$M(\Xi_c(2815))$	0.06	0.0	0.03	0.01	0.07
$M(\Xi_c(2980))$	0.14	0.0	0.12	0.05	0.2
$M(\Xi'_c)$	0.4	0.0	0.03	0.03	0.4
$M(\Xi_c(2790))$	0.06	0.0	0.04	0.05	0.1
$\Gamma(\Xi_c(2645))$	0.0	0.10	0.06	0.03	0.13
$\Gamma(\Xi_c(2815))$	0.0	0.16	0.02	0.10	0.17
$\Gamma(\Xi_c(2980)^0)$	0.0	0.1	0.7	+0.7, -1.8	+1.0, -1.8
$\Gamma(\Xi_c(2980)^+)$	0.0	0.1	0.7	+0.7, -5.0	+1.0, -5.0
$\Gamma(\Xi_c(2790))$	0.0	0.2	0.3	0.6	0.8

TABLE IV. The final results for the masses (in  $\text{MeV}/c^2$ ) and widths (in MeV) for the five isodoublets under study. For comparison, the 2015 world averages [2] (denoted “PDG”) are also quoted. Mass differences are with respect to the daughter states.

Particle	Yield	Mass	$M - M(\Xi_c)$	$M - M(\Xi'_c)$	Width
$\Xi_c(2645)^+$	$1260 \pm 40$	$2645.58 \pm 0.06 \pm 0.07^{+0.28}_{-0.40}$	$174.66 \pm 0.06 \pm 0.07$		$2.06 \pm 0.13 \pm 0.13$
PDG		$2645.9 \pm 0.5$	$175.0 \pm 0.6$		$2.6 \pm 0.2 \pm 0.4$
$\Xi_c(2645)^0$	$975 \pm 36$	$2646.43 \pm 0.07 \pm 0.07^{+0.28}_{-0.40}$	$178.46 \pm 0.07 \pm 0.07$		$2.35 \pm 0.18 \pm 0.13$
PDG		$2645.9 \pm 0.5$	$178.0 \pm 0.6$		$< 5.5$
$\Xi_c(2815)^+$	$941 \pm 35$	$2816.73 \pm 0.08 \pm 0.06^{+0.28}_{-0.40}$	$348.80 \pm 0.08 \pm 0.06$		$2.43 \pm 0.20 \pm 0.17$
PDG		$2816.6 \pm 0.9$	$348.7 \pm 0.9$		$< 3.5$
$\Xi_c(2815)^0$	$1258 \pm 40$	$2820.20 \pm 0.08 \pm 0.07^{+0.28}_{-0.40}$	$349.35 \pm 0.08 \pm 0.07$		$2.54 \pm 0.18 \pm 0.17$
PDG		$2819.6 \pm 1.2$	$348.8 \pm 1.2$		$< 6.5$
$\Xi_c(2980)^+$	$916 \pm 55$	$2966.0 \pm 0.8 \pm 0.2^{+0.3}_{-0.4}$	$498.1 \pm 0.8 \pm 0.2$		$28.1 \pm 2.4^{+1.0}_{-5.0}$
PDG		$2970.7 \pm 2.2$			$17.9 \pm 3.5$
$\Xi_c(2980)^0$	$1443 \pm 75$	$2970.8 \pm 0.7 \pm 0.2^{+0.3}_{-0.4}$	$499.9 \pm 0.7 \pm 0.2$		$30.3 \pm 2.3^{+1.0}_{-1.8}$
PDG		$2968.0 \pm 2.6 \pm 0.5$			$20 \pm 7$
$\Xi_c^+$	$7055 \pm 211$	$2578.4 \pm 0.1 \pm 0.4^{+0.3}_{-0.4}$	$110.5 \pm 0.1 \pm 0.4$		
PDG		$2575.6 \pm 3.0$	$107.8 \pm 3.0$		
$\Xi_c^0$	$11560 \pm 276$	$2579.2 \pm 0.1 \pm 0.4^{+0.3}_{-0.4}$	$108.3 \pm 0.1 \pm 0.4$		
PDG		$2577.9 \pm 2.9$	$107.0 \pm 2.9$		
$\Xi_c(2790)^+$	$2231 \pm 103$	$2791.6 \pm 0.2 \pm 0.1 \pm 0.4^{+0.3}_{-0.4}$	$320.7 \pm 0.2 \pm 0.1 \pm 0.4$	$213.2 \pm 0.2 \pm 0.1$	$8.9 \pm 0.6 \pm 0.8$
PDG		$2789.8 \pm 3.2$	$318.2 \pm 3.2$		$< 15$
$\Xi_c(2790)^0$	$1241 \pm 72$	$2794.9 \pm 0.3 \pm 0.1 \pm 0.4^{+0.3}_{-0.4}$	$323.8 \pm 0.2 \pm 0.1 \pm 0.4$	$215.7 \pm 0.2 \pm 0.1$	$10.0 \pm 0.7 \pm 0.8$
PDG		$2791.9 \pm 3.3$	$324.0 \pm 3.3$		$< 12$

of the masses of the ground states become available.

## COMPARISONS WITH THEORETICAL MODELS

Of the five excited  $\Xi_c$  isodoublets investigated here, there are clear spin-parity assignments for four of them. The exception is the copiously produced  $\Xi_c(2980)$ . The evidence presented here that the  $\Xi_c(2980)$  states decay significantly to  $\Xi'_c \pi^+$  may be used to clarify the situation. We note that the  $\Xi_c(2980)$  may be the strange analog of the  $\Lambda_c(2765)$ , which also has a high cross section, and appears to decay to  $\Sigma_c(2455)$  and  $\Sigma_c(2520)$  [21, 22]. A possible interpretation of these states is that they represent radial excitations of the ground-state charmed baryons [23].

Many models relate the intrinsic widths of the particles in the charmed baryon spectrum. The strange charmed sector and the non-strange charmed sector (*i.e.*  $\Lambda_c/\Sigma_c$ ) give complementary information on what, in HQS, are the same coupling constants. For instance, using the input from the measurement of the  $\Lambda_c^+(2595)$  width [2] leads to

TABLE V. The isospin splitting between the members of each isodoublet.

Particle	$M(\Xi_c^+) - M(\Xi_c^0)$ (MeV/ $c^2$ )
$\Xi_c(2645)$	$-0.85 \pm 0.09 \pm 0.08 \pm 0.48$
$\Xi_c(2815)$	$-3.47 \pm 0.12 \pm 0.05 \pm 0.48$
$\Xi_c(2980)$	$-4.8 \pm 0.1 \pm 0.2 \pm 0.5$
$\Xi'_c$	$-0.8 \pm 0.1 \pm 0.1 \pm 0.5$
$\Xi_c(2790)$	$-3.3 \pm 0.4 \pm 0.1 \pm 0.5$

predictions of the intrinsic width of the  $\Xi_c(2790)$  baryons. However, those measurements are complicated by the fact that the  $\Lambda_c^+(2595) \rightarrow \Sigma_c \pi$  decay occurs very close to threshold, and how exactly its mass is measured and the distortion of its line-shape is treated can greatly influence the predictions. For instance, Cheng and Chua [14], using the latest values for the  $\Lambda_c^+(2595)$ , predict  $\Gamma(\Xi_c^+(2790)) = 16.7^{+3.6}_{-3.6}$  MeV and  $\Gamma(\Xi_c^0(2790)) = 17.7^{+2.9}_{-3.8}$  MeV, whereas, using earlier values, they found  $\Gamma(\Xi_c^+(2790)) = 8.0^{+4.7}_{-3.3}$  MeV and  $\Gamma(\Xi_c^0(2790)) = 8.5^{+5.0}_{-3.5}$  MeV, which are very close to our experimental measurements. The measurements of the  $\Xi_c(2790)$  states allow far more robust measurements of the coupling constants to be made.

Similarly, the measurements of  $\Xi_c(2815)$  widths are in reasonable agreement with some previous predictions [25, 26], but less so with Cheng and Chua's latest model that predicts  $\Gamma \approx 7.4$  MeV [14]. The analogous decay to  $\Xi_c(2815) \rightarrow \Xi_c(2645)\pi$  in the  $\Lambda_c/\Sigma_c$  sector is  $\Lambda_c^+(2625) \rightarrow \Sigma_c(2520)\pi$  which is not kinematically allowed, again complicating the extraction of the relevant parameters.

The measurements of the widths of the  $\Xi_c(2645)$  baryons are in good agreement with calculations. Here the predictions are more robust as they rely upon the measurements of the  $\Sigma_c^{++}$  and  $\Sigma_c^0$  baryons, which have closely analogous decays. Using the recent high-precision values of  $\Sigma_c$  widths [19], Cheng and Chua predict  $\Gamma(\Xi_c^+(2645)) = 2.4^{+0.1}_{-0.2}$  MeV and  $\Gamma(\Xi_c^0(2645)) = 2.5^{+0.1}_{-0.2}$  MeV, close to our new measurements, further validating the use of HQS in the charm sector.

The isospin splittings of charmed baryons are due to the difference in the  $u$  and  $d$  quark masses together with electromagnetic interactions. In 2003 several versions of non-relativistic quark model [27] predicted small ( $< 1$  MeV/ $c^2$ ) splittings in the  $\Xi'_c$  and  $\Xi_c(2645)$  systems, but a splitting of  $\approx 3$  MeV/ $c^2$  in the  $\Xi_c(2815)$  system, similar to the ground states and in good agreement with the results presented here. The sizeable measured splittings of the  $\Xi_c^+(2980)$  and  $\Xi_c^0(2980)$  may help to identify the states. The  $\Xi'_c$  system has been the subject of some theoretical interest, and several authors [28] predict small negative isospin splittings, in agreement with our measurements.

## SUMMARY AND CONCLUSIONS

Using the entire 980 fb $^{-1}$  of data recorded by the Belle detector at the KEKB  $e^+e^-$  collider operating in the  $\Upsilon$  energy range, we present new measurements of the masses of all members of five isodoublets of excited  $\Xi_c$  states, and intrinsic widths of those that decay strongly. Of the eighteen measurements, five are of intrinsic widths of particles for which only limits existed previously. Of the remaining thirteen measurements, ten are within one standard deviation of the Particle Data Group [2] best-fit values. The three measurements that are in modest disagreement with previous results are in the  $\Xi_c(2980)$  sector, where the previous measurements were dominated by decays into different final states and for which some measurements may have been prone to the existence of more than one resonance in the region, or biases from threshold effects. Although some of the previous measurements were made by Belle, they are all essentially independent of those presented here. For instance, although the measurement of  $\Gamma(\Xi_c^+(2645))$  was made with the same dataset, it was made using only three decay modes of the  $\Xi_c^0$  but without the  $\Xi_c(2815)$  tag, and the limiting systematic uncertainties are from completely different sources, thus making the measurements effectively complementary.

The intrinsic width measurements of the  $\Xi_c(2790)$  and  $\Xi_c(2815)$  states present a consistent picture with the intrinsic widths that can be related to measurements in the  $\Lambda_c/\Sigma_c$  system and used to predict measurements in the  $b$ -hadron sector. The mass measurements constitute a considerable improvement in precision on previous measurements, and allow further investigation of hadron mass models including isospin splittings.

We thank the KEKB group for the excellent operation of the accelerator; the KEK cryogenics group for the efficient operation of the solenoid; and the KEK computer group, the National Institute of Informatics, and the PNNL/EMSL computing group for valuable computing and SINET4 network support. We acknowledge support from the Ministry of Education, Culture, Sports, Science, and Technology (MEXT) of Japan, the Japan Society for the Promotion of Science (JSPS), and the Tau-Lepton Physics Research Center of Nagoya University; the Australian Research Council; Austrian Science Fund under Grant No. P 22742-N16 and P 26794-N20; the National Natural Science

Foundation of China under Contracts No. 10575109, No. 10775142, No. 10875115, No. 11175187, No. 11475187 and No. 11575017; the Chinese Academy of Science Center for Excellence in Particle Physics; the Ministry of Education, Youth and Sports of the Czech Republic under Contract No. LG14034; the Carl Zeiss Foundation, the Deutsche Forschungsgemeinschaft, the Excellence Cluster Universe, and the VolkswagenStiftung; the Department of Science and Technology of India; the Istituto Nazionale di Fisica Nucleare of Italy; the WCU program of the Ministry of Education, National Research Foundation (NRF) of Korea Grants No. 2011-0029457, No. 2012-0008143, No. 2012R1A1A2008330, No. 2013R1A1A3007772, No. 2014R1A2A2A01005286, No. 2014R1A2A2A01002734, No. 2015R1A2A2A01003280 , No. 2015H1A2A1033649; the Basic Research Lab program under NRF Grant No. KRF-2011-0020333, Center for Korean J-PARC Users, No. NRF-2013K1A3A7A06056592; the Brain Korea 21-Plus program and Radiation Science Research Institute; the Polish Ministry of Science and Higher Education and the National Science Center; the Ministry of Education and Science of the Russian Federation and the Russian Foundation for Basic Research; the Slovenian Research Agency; Ikerbasque, Basque Foundation for Science and the Euskal Herriko Unibertsitatea (UPV/EHU) under program UFI 11/55 (Spain); the Swiss National Science Foundation; the Ministry of Education and the Ministry of Science and Technology of Taiwan; and the U.S. Department of Energy and the National Science Foundation. This work is supported by a Grant-in-Aid from MEXT for Science Research in a Priority Area (“New Development of Flavor Physics”) and from JSPS for Creative Scientific Research (“Evolution of Tau-lepton Physics”).

- 
- [1] Throughout this paper, the inclusion of the charge-conjugate mode decay is implied unless otherwise stated.
  - [2] K. Olive *et al.* (Particle Data Group), Chin. Phys. **C38**, 090001 (2014) and 2015 update.
  - [3] R. Chistov *et al.* (Belle Collaboration), Phys. Rev. Lett. **97**, 162001 (2006).
  - [4] B. Aubert *et al.* (BaBar Collaboration), Phys. Rev. D **77**, 012002 (2008).
  - [5] Y. Kato *et al.* (Belle Collaboration), Phys. Rev. D **89**, 052003 (2014).
  - [6] Y. Kato *et al.* (Belle Collaboration), arXiv:1605.09103 (2016), submitted to Phys. Rev. D.
  - [7] N. Isgur and M. B. Wise, Phys. Rev. Lett. **66**, 1130 (1991).
  - [8] C.P. Jessop *et al.* (CLEO Collaboration), Phys. Rev. Lett. **82**, 492 (1999).
  - [9] P. Avery *et al.* (CLEO Collaboration), Phys. Rev. Lett. **75**, 4364 (1995).
  - [10] L. Gibbons *et al.* (CLEO Collaboration), Phys. Rev. Lett. **77**, 810 (1996).
  - [11] S. Csorna *et al.* (CLEO Collaboration), Phys. Rev. Lett. **86**, 4243 (2001).
  - [12] J. Alexander *et al.* (CLEO Collaboration), Phys. Rev. Lett. **83**, 3390 (1999).
  - [13] T. Lesiak *et al.* (Belle Collaboration), Phys. Lett. B **655**, 9 (2008).
  - [14] H.-Y. Cheng and C.-K. Chua, Phys. Rev. D **92**, 074014 (2015).
  - [15] A. Abashian *et al.* (Belle Collab.), Nucl. Instr. and Meth. A **479**, 117 (2002); see also detector section in J. Brodzicka *et al.*, Prog. Theor. Exp. Phys. **2012**, 04D001 (2012).
  - [16] S. Kurokawa and E. Kikutani, Nucl. Instr. and Meth. A **499**, 1 (2003), and other papers included in this volume.
  - [17] D. Lange, Nucl. Instr. Meth. A **462**, 152 (2001).
  - [18] R. Brun *et al.* GEANT3.21, CERN Report DD/EE/84-1 (1984).
  - [19] S. H. Lee *et al.* (Belle Collaboration), Phys. Rev. D **89**, 091102 (2014).
  - [20] T. Skwarnicki, Ph.D. Thesis, Institute for Nuclear Physics, Krakow 1986; DESY Internal report, DESY F31-86-02 (1986).
  - [21] M. Artuso *et al.* (CLEO Collaboration), Phys. Rev. Lett. **86**, 4479 (2001).
  - [22] C.W. Joo, representing the Belle Collaboration, PoS(Hadron2013), 210 (2013).
  - [23] D. Ebert, R. N. Faustov and V. O. Galkin, Phys. Rev. D **84**, 014025 (2011); B. Chen, K. Wei and A. Zhang, Eur. Phys. J. A **51** 82 (2015).
  - [24] <https://root.cern.ch/roofit>.
  - [25] H.-Y. Cheng and C.-K. Chua, Phys. Rev. D **75**, 014006 (2007).
  - [26] S. Tawfiq, J. Korner, V. Lyubovitskij and A. Rusetsky, Phys. Rev. D **55**, 7317 (1997).
  - [27] B. Silvestre-Brac, F. Brau, and C. Semay, J. Phys. G **29**, 2685 (2003).
  - [28] F.-K. Guo, C. Hanhart and U.-G. Meissner, JHEP **0809** 136 (2008).